ANALOG MICRO DELTA (μΔ) MOTOR: COMPLIANT MECHANISM ENABLED MEMS BIDIRECTIONAL TRANSMISSION-CAPABLE GAP CLOSING ARRAY

Alexander N. Alvara[1], Yichen Liu[2], Liwei Lin[1], and Kristofer S. J. Pister[2]
[1]Department of Mechanical Engineering, University of California, Berkeley, USA
[2]Department of Electrical Engineering and Computer Sciences, University of California, Berkeley, USA

ABSTRACT

This work presents the first bidirectional transmission motor using a MEMS gap-closing actuator with a simple compliant beam bending mechanism. A continuous range of forward and reverse motions have been achieved by bending the pawl of the mechanism with a force exerted perpendicular to a spine structure via the compliant cantilever input gear shift, Δ. A study of the static loading and beam bending in the critical stages of motor actuation is conducted to confirm the motor performance criteria. Experimental results show an ability to impart output shuttle motion in the range of [1.5, 9.5] μm and [-2.9, -5.9] μm for a λ = 25° configuration and [4.2, 12.2] μm and [-1.5, -6.6] μm for a λ = 47.5° configuration, with an input force of 0.9375 mN for a 4.7 μm motor input and are corroborated by Ansys simulation.

INTRODUCTION

In MEMS actuation, significant technological advantage is placed on the ability to produce high force density, low power, inexpensive units that often serve a specific single purpose in a small package. Through this MEMS is both highly efficient at reaching production in applications for particular use and achieving such at scale. In this way, MEMS has often secured a position as the firmware of actuators, in that it serves exactly the use case it is designed for with embedded speed and force as outputs for its current and voltage inputs often with little relative spread in its designated and calibrated use range.

Here we present a monolithic actuator with embedded compliant structures that enable direct drive multi-force and -speed outputs in both forward and reverse directions for selected voltage and current inputs with the capability for increased range if voltage and current inputs are also ranged for a given gear shift input. The sweep inputs, Δ, can be shifted in micrometer ranges and the output shuttle movements have been characterized. Experimentally, two morphologies were tested with a design similar to the Penskiy inchworm motor as the actuation source [1].

In this work, each motor device is actuated both in forward and in reverse and the data shown below reflects such actuation schemes and is confirmed by Ansys simulation. **Figure 1** shows that through by first actuating the transverse gear shift, Δ, the pawl structure can be angled relative to the shuttle in either the forward or the reverse direction. Then, while in this gear shifted configuration, the gap-closing actuator (GCA) can be engaged, driving the pawl foot into the shuttle. While the pawl foot and shuttle are interlocked by their respective interlocking teeth, the pawl arm undergoes elastic deformation and loads elastic energy as a spring, driving the shuttle in either the forward or reverse direction (depending on gear shifting) as the elastic energy from the pawl arm is released during the rest of the GCA force travel and displacement. Afterwards, the pawl springs back to its unactuated position, releasing the shuttle.

MOTOR DESIGN

Electrostatic GCAs have a relatively large force but small displacement compared with comb-drive actuators. Electrostatic

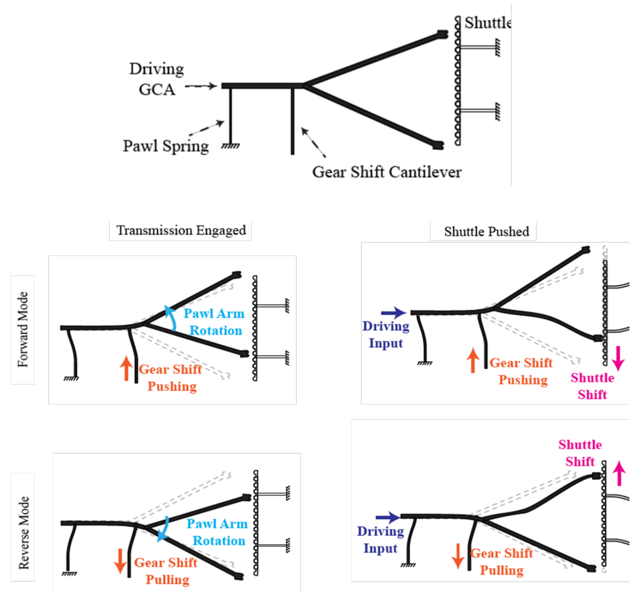

Figure 1: Diagram of the mechanics for the λ = 25° μΔ motor pawls. Top) demonstrates the initial state of the motor prior to actuation, Bottom-left) shows the gear shifted position at a given distance, Δ, (orange arrow) with the deflection angular sweep, γ, (blue arrow). Bottom-right) demonstrates the GCA driving and shuttle motion step with the bending behavior of the pawl upon contact with the shuttle showing the force transmission from the axial direction (blue arrow) the orthogonal shuttle direction (red arrow). Indicated on top is the forward and the bottom the reverse gearing with bending indicated.

inchworm motors (EIMs) overcome the small displacement by taking multiple, usually consecutive, small steps. The force from the GCA is applied to a pawl which makes repeated contact with a shuttle, moving the shuttle a small amount each time the GCA closes.

The first EIMs used two GCAs: one to engage the pawl shoe with the shuttle, and one to drive the pawl forward [2]. Hollar et al. improved on this design by making the drive GCA bi-directional, allowing the EIM to move the shuttle either forward or backward using the same drive GCA [3]. Penskiy et al. improved on the original EIM by using an angled arm, or pawl, to support the shoe [1]. This removed the need for the pawl-engagement GCA, as the main drive GCA served to both engage the pawl and move the shuttle forward. This was an improvement in simplicity and reduced the number of control signals needed for the motor, but it did prevent the use of the Hollar bidirectional GCA.

In this work, we demonstrate that by re-introducing a second displacement input, Δ, the angle of the pawl can be changed dynamically during motor operation. Penskiy showed that there was a tradeoff between shuttle output force and shuttle displacement based on the angle of the pawl [1]. By changing the

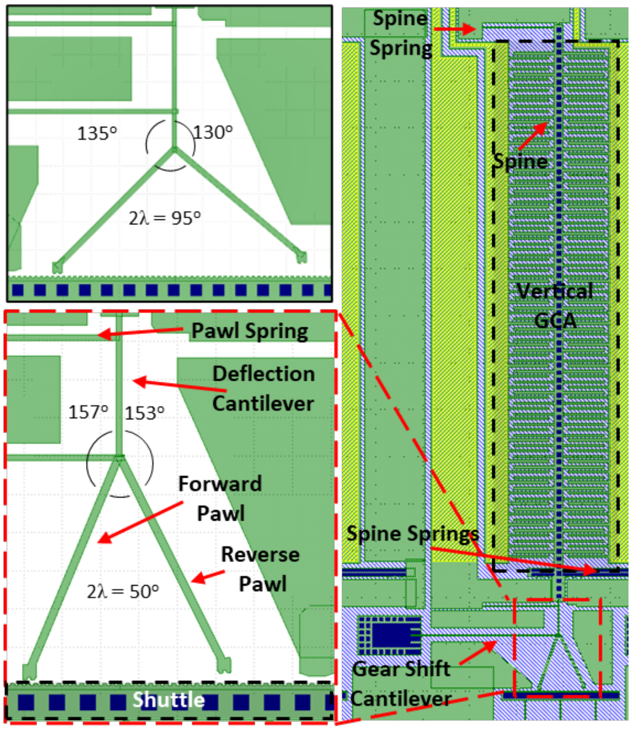

Figure 2: Diagram showing the μΔ motor (right). Left-top showing the pawl separation half-angle λ = 47.5º and left-bottom showing λ = 25º. The forward pawl of the λ = 25º device has the same angular morphology of the Penskiy pawl with the noted difference of having a reverse pawl and a gear shift cantilever attached at the meeting of the forward and reverse pawls. The distance between the pawl top and the pawl spring has been elongated for the insertion of a deflection cantilever for rotation.

angle of the pawl, this work allows that tradeoff to be made dynamically, like shifting gears on a bike. In addition, we demonstrate that a dual-pawl head can be used on the GCA (**Fig. 2**), enabling both forward and reverse motion of the shuttle.

The gear shift cantilever travels transversely and bends the pawl cantilever around the spine structure, as seen in **figure 1**. **Figure 2** shows the basic geometric structure, where the Δ shift is highlighted by using a design with a pawl structure consisting of two cantilevers with a pitch angle, λ, of 47.5º and 25º. An inverted "Y"-shaped holds a pair of pawls with notched teeth at their ends for forward and backward motions, respectively, while the other pawl idles, as seen in **figure 3**.

EXPERIMENTAL SETUP

Figure 4 shows the pitch offset that contributes to pawl tooth misalignment and subsequent shuttle motion, where offsets can impart misalignment that together with spring load on the pawl either contribute constructively or destructively to the overall shuttle motion. As the pawl gap, g_p, decreases with increasing $\delta\gamma$, the work done on the shuttle by the GCA increases thereby increasing shuttle motion. When taken together with the information from figure 4, this implies that the *μΔ-motors* not only increase the range of GCA action on the spine and therefore the pawl but also increases the range that the pawl is in contact with the shuttle adding to the work done on the shuttle in two ways.

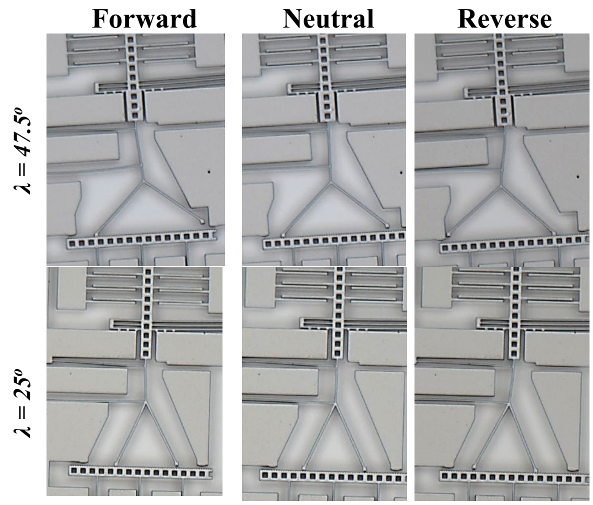

Figure 3: Optical images of fabricated devices in their actuated positions for representative display of the relative forward, neutral, and reverse positions for the 25º and 47.5º devices. In "forward gear", the left pawl pushes the shuttle left. In "reverse

MECHANICAL ANALYSIS

Compliant Structures

The shuttles have 3 cantilever springs together with $k_{sp} =$ 0.264 N/m ($l_{sp} = 220$µm, $w_{sp} = 3.5$µm, $N = 3$; or $k_{sp} = 0.928$ N/m as drawn). Each vertical gap closing array has 40 individual capacitive plate pairs attached to a single spine which together can produce approximately 0.9 mN of force under an input bias voltage of 100 V ($N = 40$, $l_{OL} = 76.2$ µm, $g_{GCA,0} = 4.9$ µm) [4, 5]. Each of the following experience simple beam bending loaded conditions: gear shift, deflection, and pawl beams. The only beams which experience higher order bending is the gear shift horizontal alignment and the pawl and spine return beams, which are not discussed as they are simple bending beams which do not contribute directly to the main compliant structures which influence the transmission capability of the µΔ-motors. Within the proper working range of normal prescribed function, simple beam bending can be expected in each of the components of the

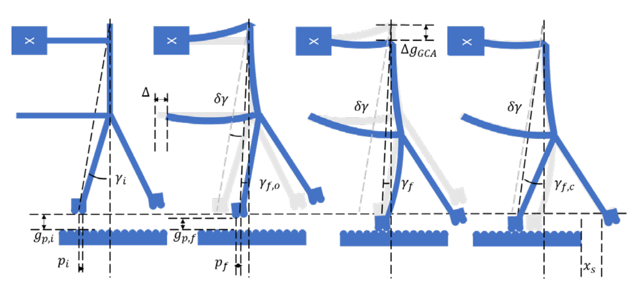

Figure 4: Diagram of small angle approximation for change in deflection angle, δγ due to Δ; the pitch offset, p, that contributes to pawl/shuttle tooth misalignment; pawl gap, g_p,which decreases with increasing δγ; and shuttle motion, x_s, which is grows with increasing work done on the shuttle due to the decrease in g_p. From left to right is the progression actuation of as fabricated, gear shifted, GCA drive input, and shuttle motion. Not to scale. Interestingly at some γ's the $x_s/\Delta g_{GCA} > 1$. Shaded grey images correspond to the previous action for reference.

compliant structure. **Figure 4** depicts the beam bending during the critical steps.

Ansys Simulations

We conduct a finite element analysis on the compliant structure comprising the gear shift cantilever, forward/reverse pawls, GCA spine, and shuttle system, illustrated in **figure 2**. In the first stage of the simulation, the gears shift cantilever displaces by 10 µm with a step size of 1 µm, while the rest of the system remains anchored near the spine and pawl springs. The forward/reverse pawls deform under the static load induced by the gear shift cantilever displacement. Subsequently, the spine displaces by 3.8µm in the vertical direction and returns to its neutral state at each step of gear shifting displacement, simulating the GCA actuation. The forward pawl's tip moves toward the shuttle until contact occurs between the pawl teeth and shuttle teeth. The shuttle displacement serves as the output of the compliant structure. Ansys simulation set up shown in **figure 5**.

First, we examine the response of the complaint structure with gear-shifting displacement only. As the input displacement increases at the end of the gear shift beam, the system rotates counterclockwise. As a result, the GCA spine displaces upward locally changing the effective initial gap and different pull-in voltage is needed at simulation step. The values for the pull in voltage were estimated using the below equations:

$$V_{PI} = \sqrt{\frac{8}{27}\frac{k_{eq} g_0^3}{\epsilon_0 A}} \tag{1}$$

where k_{eq} is the equivalent stiffness of the complaint system in vertical GCA direction, g_0 is the initial gap between GCA fingers, ϵ_0 is the permittivity of free space, and A is the total overlapping area between the GCA fingers. The complaint structure is connected to four clamp-clamped springs along y-axis in parallel: gear shifting beam, spine springs, and the pawl spring, as called-out in **figure 2**. Therefore, the effective stiffness, k_{eq} , is the sum of the stiffness all four clamp-clamp spring systems where induvial stiffness is described by equation (##)

$$k = \frac{Ewt^3}{L^3} \tag{2}$$

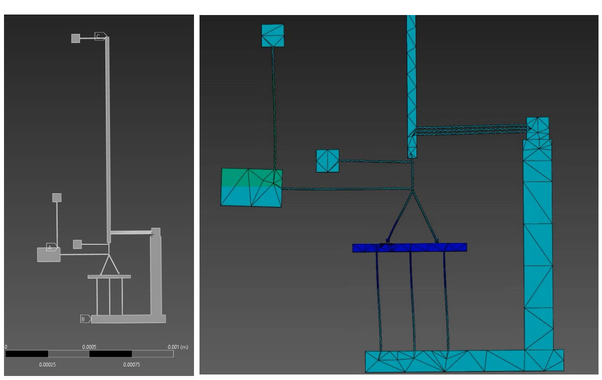

Figure 5: Left showing the full problem set-up with scale bar of 1 mm. Right showing the actuated deflection of the shuttle and GCA µΔ motor. Shown shuttle movement is 8 µm with a 4 µm gear shift input distance.

where E is the Young's modulus of the material and w, t, L are the width, thickness, and length of the beam respectively. The resulting pull-in voltage versus input gear shifting displacement is presented in the results section by **figure 6** and **figure 7**.

We then examine the system response to the GCA stride at each step of the gear shifting displacement. Both the initial distance and attack angle between the forward/reverse pawl and the shuttle change because of the gear shifting displacement. The initial distance between the pawl tip and shuttle determines the effective travel of the GCA that can contribute to the shuttle deformation. The attack angle determines the ratio of GCA output force that is converted into the thrust displacing shuttle along the x axis versus the normal force between the pawl tip and shuttle interface. As a result of both factors, the maximum distance the shuttle travels change at each gear shifting displacement as shown in **figure 7**. When gear shifting input is low, shuttle displacement is dominated by the initial gap between the pawl tip and shuttle teeth; GCA displacement must overcome the large initial gap and not enough thrust is converted to shuttle displacement. At a large gear shifting input, however, the attack angle between pawl teeth and shuttle dominates the shuttle displacement.

Video Analysis

Videos of the moving compliant system were captured for both narrow (λ=25°) and wide (λ=47.5°) devices. A probe station pin was employed to manually switch gears by displacing the gear shift cantilever. The vertical GCAs were driven at a frequency of 10 Hz, and the resulting shuttle displacement was recorded. Positions of points of interest were sampled for each device: the end of the gear shift cantilever, the shuttle, the tips of the forward and reverse pawls, the junction of the forward/reverse pawls, and the junction of spine deflection with the cantilever.

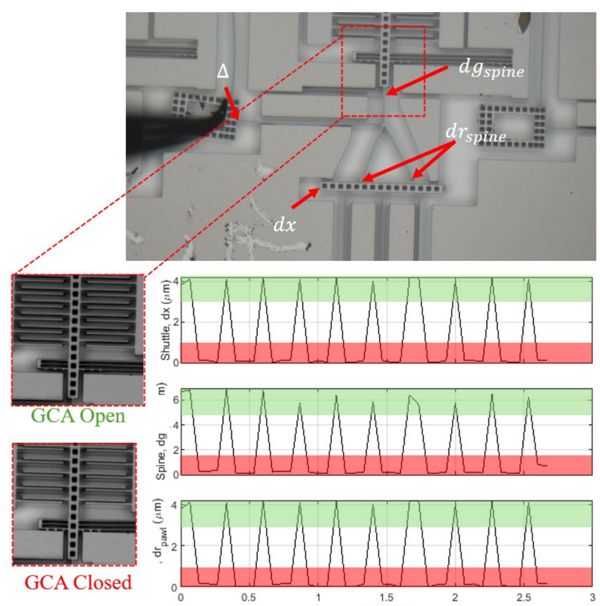

Figure 6: Top) Diagram showing the video capture software indicating open and closed positions in the insets. Bottom) Time-plots of the indicated shuttle, spine, and pawl motion for reference.

FABRICATION AND CHARACTERIZATION

The fabrication is a standard 3-mask metal on SOI wafer. Starting with a substrate (550 µm), oxide (2 µm), device (40 µm), a deposition of standard MIR 701 PR (2 µm) with the Picotrack PCT- 150 CRS, lithography using the Heidelberg

Maskless Aligner 150. Metal deposition of Cr (100 nm), for adhesion, and Au (100nm), for oxide protection, is accomplished with the CHA e-beam evaporator. DRIE is accomplished using the Silicon Technologies Services (STS2 ICP SR), hard baking using timed UV lamp via the Axcelis M200PCU Photostabilizer. PR ash is accomplished with the

RESULTS

Figure 7 shows the Ansys results which correspond to the forward, between 1 to 10 μm, and parts of the reverse gear shifted, between 1 to 10 μm, actuation performance. The magnitude of shuttle motion increases as the gear shifting displacement increases in both forward and reverse direction. We observe an asymmetrical change in shuttle motion near zero input as the gear shift overcomes the as-fabricated forward state. Spine motion due to the rotation of the compliant structure with increasing gear shift changes the initial gap of the GCAs in a linear trend between 1 to 10 μm of displacement with its corresponding pull -in voltage.

The video analysis results are indicated in **figure 8**, where the software, indicated in **figure 6**, is used to extract the relative positions of the individual components of the critical structure. The observed pull-in voltage and shuttle displacement agrees with the simulated value.

The GCA pull-in voltage variation is different for each Δ input, as seen in **figure 9**. This variation is attributed to the shift cantilever compliant mechanism, which increases the stiffness in the pawl imparting a decrease of GCA gap distance, g_{GCA}, prior to actuation in the reverse and an increase in the forward direction.

Mechanical characterization, indicated in **figure 10**, shows a monotonic relationship between μm-scale deflection angle, γ, and the shuttle motion. While the shuttle does not constitute a force test, the distance the shuttle is pushed corresponds to range of output motion in the Δ shift for the given stiffness close to the no-load condition.

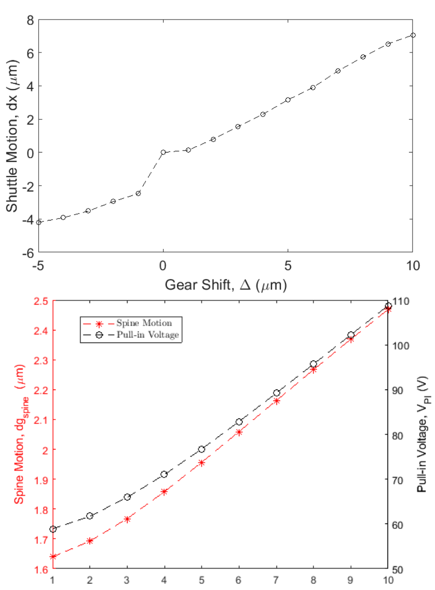

Figure 7: Top) Shuttle motion vs. gear shift for $\lambda = 25°$ configuration in ANSYS simulations. Bottom) Spine motion and its corresponding pull-in voltage vs. gear shift

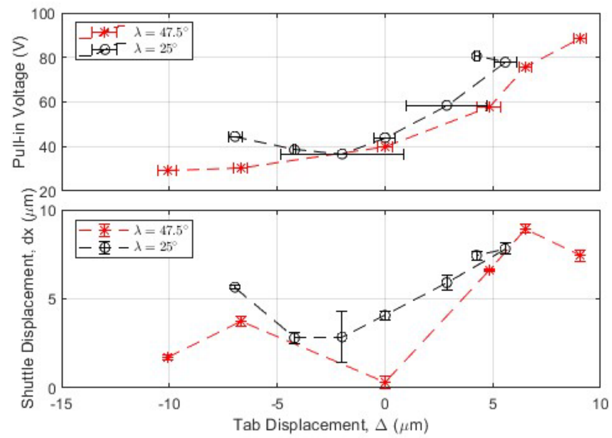

Figure 8: Video analysis capture data for Top) pull-in voltage (V_{PI}) vs gear shift position (Δ) and Bottom) shuttle displacement (dx) vs gear shift position (Δ).

CONCLUSIONS

This work demonstrates the capabilities for an analog microscale transmission motor with the compliant beam bending design for microscale robotics. It presents the near no-load condition for a mechanism for shifting between geared positions for varied force and distance outputs without using separate controlling devices. The output displacement of the shuttle is nearly three times the GCA travel and more than twice that of the original Penskiy motors, indicating that the overall gear shift mechanism is of high effective performance in the static case. Future work will encompass dynamic analysis of the analog μΔ-motors, a recently designed digital μΔ-motor, and design which mixes elements of the two, termed the digilog μΔ-motor. This work will also encompass microrobot integration and overall mechanical performance in an application specific goal-case.

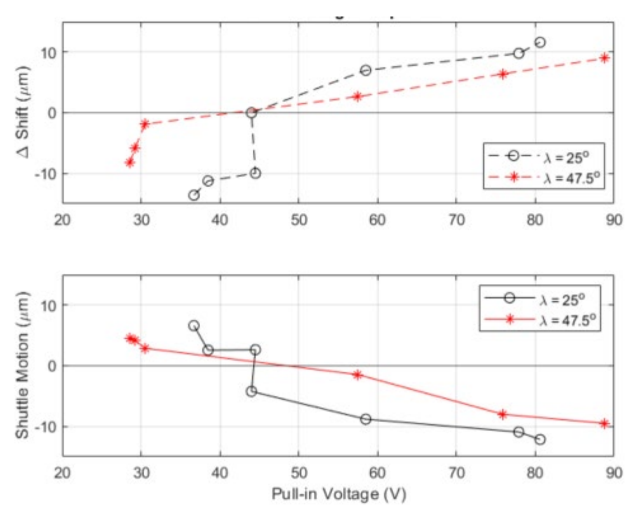

Figure 9: Plot of experimental data of Top) gear shift position (Δ) vs pull-in voltage (V_{PI}) and Bottom) shuttle motion (dx) vs pull in voltage (V_{PI}) for the λ = 47.5° and λ = 25° devices. The trend for change in pull in voltage is explained by the shift in finger gaps owed to the compliant beam bending which closes the fingers more in the reverse direction and opens them more in the forward direction.

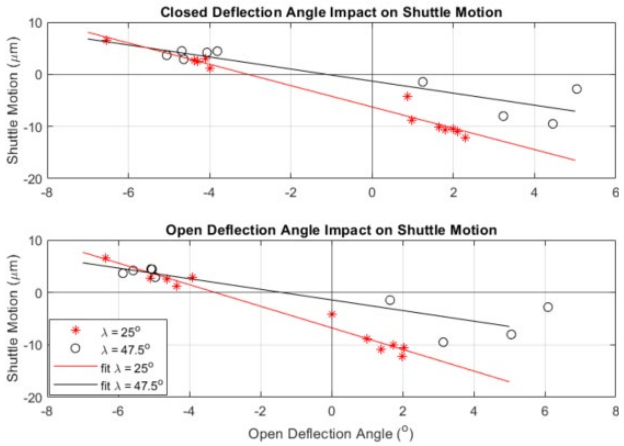

Figure 10: Plot of experimental data of shuttle motion vs Top) open and Bottom) closed deflection angle, γ. The plots show the shift in delta angle from the open to closed position of the GCA fingers owed to the bending in the compliant beams, top showing the λ = 25° and bottom showing the λ = 47.5° configurations. Note: while the open deflection angle does not cause a shuttle motion it is in the action space of the given shuttle motion value plotted and should be considered a pre-shuttle engagement value. This is given to emphasize the strain energy transmitted from pawl to shuttle.

ACKNOWLEDGEMENTS

The authors would like to thank the staff of the UC Berkeley Marvell Nanolab for continued support and discussions around fabrication. This project was accomplished in part with funding from the National Science Foundation Graduate Research Fellowship Program (NSF-GRFP), the National GEM Fellowship, the Ford Predoctoral Fellowship, the Robert P. Lin SSL Fellowship, and the Diversity & Community Fellowships. Special thanks to Daniel Lovell, Daniel Teal, and Daniel Klawson for their contributions to discussion and previous works that helped immensely as well as their dedication to the graduate student community.

REFERENCES

1. I. Penskiy and S. Bergbreiter, "Optimized Electrostatic Inchworm Motors Using a Flexible Driving Arm," *Journal of Micromechanics and Microengineering*, 23, 1 (2012).
2. R. Yeh, S. Hollar, and K. S. J. Pister. 2002. "Single mask, large force and large displacement electrostatic linear inchworm motors." *J. Microelectromech. Syst.* 11 330–6
3. S. Hollar, S. Bergbreiter, and K. S. J. Pister, "Bidirectional Inchworm Motors and Two-DOF Robot Leg Operation," *International Conference on Solid-State Sensors, Actuators, and Microsystems (Transducers)*, 1, 262-267 (2003).
4. A. Rauf, D. S. Contreras, R. M. Shih, C. B. Schindler, and K. S. J. Pister, "Nonlinear Dynamics of Lateral Electrostatic Gap Closing Actuators for Applications in Inchworm Motors," *Journal of Microelectromechanical Systems*, 31, 1 (2022).
5. C. B. Schindler, H. C. Gomez, and K. S. J. Pister, "First Jumps of a Silicon Microrobot with an Energy Storing Substrate Spring," *International Conference on Solid-State Sensors, Actuators, and Microsystems (Transducers)*, 1, 349-352 (2021).

CONTACT

*A. N. Alvara, engineer_alvara@berkeley.edu